INTERNATIONAL JOURNAL FOR NUMERICAL METHODS IN FLUIDS, VOL. 13, 917–936 (1991)

MAGNETOHYDRODYNAMIC STEADY FLOW COMPUTATIONS IN THREE DIMENSIONS

SEUNGSOO LEE* AND GEORGE S. DULIKRAVICH

Aerospace Engineering Department, The Pennsylvania State University, University Park, PA 16802, U.S.A.

SUMMARY

A complete three-dimensional mathematical model has been developed governing the steady, laminar flow of an incompressible fluid subjected to a magnetic field and including internal heating due to the Joule effect, heat transfer due to conduction, and thermally induced buoyancy forces. The thermally induced buoyancy was accounted for via the Boussinesq approximation. The entire system of eight partial differential equations was solved by integrating intermittently a system of five fluid flow equations and a system of three magnetic field equations and transferring the information through source-like terms. An explicit Runge–Kutta time-stepping algorithm and a finite difference scheme with artificial compressibility were used in the general non-orthogonal curvilinear boundary-conforming co-ordinate system. Comparison of computational results and known analytical solutions in two and three dimensions demonstrates high accuracy and smooth monotone convergence of the iterative algorithm. Results of test cases with thermally induced buoyancy demonstrate the stabilizing effect of the magnetic field on the recirculating flows.

KEY WORDS Magnetohydrodynamics CFD Thermal buoyancy Iterative algorithms Explicit algorithms

INTRODUCTION

It is a well-known fact that a magnetic field has a strong effect on fluid flows. For example, a Poiseuille velocity profile flattens owing to the applied magnetic field. In the presence of the magnetic field the strengths of vortices produced by thermal instability can be reduced. Engineers have used the properties of the magnetic field in applications ranging from flowmeters to space processing.

Despite its importance in engineering aplications, only a few attempts[1,2] have been made to simulate magnetohydrodynamic phenomena numerically. However, these works were restricted to two-dimensional problems. In the present paper a complete three-dimensional numerical simulation of steady, laminar, magnetohydrodynamic incompressible flow was performed, although the numerical procedure can be extended to unsteady and compressible flows. The first part of this paper presents a mathematical model of magnetohydrodynamics. The electric field vector is eliminated from the Maxwell equations using Joule's law. This results in magnetic transport equations which consist of three partial differential equations of mixed hyperbolic–parabolic type. These magnetic transport equations are integrated along with the Navier–Stokes equations. The second part of the paper presents the numerical method for solving the system of governing equations. The system of equations is split into two systems of equations:

* Presently with Agency for Defense Development, Daejon, Korea.

0271-2091/91/170917-20$10.00

Received 18 June 1990
Revised 24 January 1991

the system for the fluid flow field and the system for the magnetic field. Such a splitting approach was used by a number of researchers to solve the Navier–Stokes equations with the k–ε equations of turbulence.[3,4] One of the advantages of this approach is that additional equations (turbulence, magnetic field, etc.) can be included without modifying the existing basic flow solver. On the other hand, a slightly adverse effect on numerical stability could be expected as the result of partially 'decoupling' the global system.

A stability analysis of this approach was performed in conjunction with an explicit Runge–Kutta method. The stability analysis was performed by considering an equivalent multistage scheme similar to the split Runge–Kutta procedure. Stability results show that the split procedure does not change the stability of the global scheme significantly. As long as the CFL condition for each individual system is separately satisfied, the stability condition for the split approach is satisfied.

GOVERNING EQUATIONS

After ignoring the electric displacement vector, Maxwell's equations[5] can be written in Cartesian tensor notation as

$$H_{i,i}=0, \tag{1}$$

$$\varepsilon_{ijk}H_{k,j}=\frac{4\pi}{c}J_i, \tag{2}$$

$$\varepsilon_{ijk}E_{k,j}=-\frac{\mu}{c}H_{i,t}, \tag{3}$$

where ε_{ijk} is the permutation symbol and commas designate differentiation. Here H_i and E_i are the components of the magnetic field vector and the electric field vector, while c, μ and t are the speed of light, the magnetic permeability and time, respectively. The equations are cast in Gaussian units and the repeated index denotes summation over the index. Joule's law is given by

$$J_i=\sigma\left(E_i+\frac{\mu}{c}\varepsilon_{ijk}v_jH_k\right) \tag{4}$$

where J_i and v_i are the components of the electric current density vector and the fluid velocity vector respectively. The coefficient σ is the electrical conductivity.

With the aid of the Boussinesq approximation[6] the Navier–Stokes equations for the incompressible electrically conducting homocompositional fluid flow including buoyancy force are given by mass conservation,

$$v_{i,i}=0, \tag{5}$$

momentum conservation,

$$v_{i,t}+(v_iv_j)_{,j}=-\frac{1}{\rho}p_{,i}+\frac{\eta}{\rho}v_{,jj}+\frac{\mu}{c\rho}\varepsilon_{ijk}J_jH_k-\alpha g_i(T-T_c), \tag{6}$$

and energy conservation,

$$T_{,t}+(v_jT)_{,j}=\kappa T_{,jj}+\frac{J_jJ_j}{\rho\sigma c_p}, \tag{7}$$

where g_i, ρ, p and T are the gravity components, the fluid density, the sum of hydrodynamic and hydrostatic pressure and the temperature respectively. Here η, α, κ and c_p are the coefficients of

viscosity, thermal expansion, thermal diffusivity and specific heat respectively. The third term on the right-hand side of the momentum equation is the Lorentz force due to the magnetic field. The last term on the right-hand side of the momentum equation is the thermal buoyancy force. Notice that the viscous dissipation terms are neglected, while the Joule heating is included in the energy equation in accordance with the Boussinesq approximation.

Eliminating E_i between the Maxwell equations (1)–(3), we have the so-called magnetic transport equation

$$H_{i,t}-(v_jH_i-v_iH_j)_{,j}=\frac{c^2}{4\pi\mu\sigma}H_{i,jj}. \tag{8}$$

From the definition of the electric density vector, equation (4), and the vector identities, the momentum equation (6) can be written as

$$v_{i,t}+\left(v_iv_j-\frac{\mu}{4\pi}H_iH_j\right)_{,j}=-\frac{1}{\rho}p^*_{,i}+\frac{\eta}{\rho}v_{i,jj}-\alpha g_i(T-T_c), \tag{9}$$

where the combination of hydrostatic, hydrodynamic and magnetic field pressure is

$$p^*=p+\frac{\mu H_iH_j}{8\pi}. \tag{10}$$

For convenience the superscript asterisk will be dropped.

NON-DIMENSIONALIZATION

It is desirable to non-dimensionalize the governing equations in order to simplify the study of the relative importance of each physical phenomenon involved. The following non-dimensional form of the governing equations is obtained:

$$v_{i,i}=0, \tag{11}$$

$$v_{i,t}+\left(v_iv_j-\frac{Ht}{RmRe}H_iH_j\right)_{,j}=-p_{,i}+\frac{1}{Re}v_{i,jj}-\frac{Gr}{Re^2}e_i\theta, \tag{12}$$

$$\theta_{,t}+(v_j\theta)_{,j}=\frac{1}{PrRe}\theta_{,jj}-\varepsilon_m, \tag{13}$$

$$H_{i,t}-(v_jH_i-v_iH_j)_{,j}=\frac{1}{Rm}H_{i,jj}. \tag{14}$$

Here θ is the normalized temperature, $(T-T_c)/\Delta T$, and $\Delta T=T_h-T_c$, where T_h and T_c are two reference temperatures. The unit vector in the direction of the gravitational vector is designated as e_i. The term due to Joule heating becomes

$$\varepsilon_m=\frac{EcHt^2}{Rm^2Re}\varepsilon_{ijk}\varepsilon_{ilm}H_{k,j}H_{m,l} \tag{15}$$

and the non-dimensional numbers are given by

Eckert number $$Ec=\frac{v_r^2}{c_p\Delta T},$$

Grashof number $$Gr=\frac{\rho\alpha g l_r^3\Delta T}{\eta^2}.$$

Hartman number $$Ht=\mu l_r H_r\sqrt{\left(\frac{\sigma}{c^2\eta}\right)},$$

Magnetic Reynolds number $$Rm=RePm=\frac{4\pi\mu\sigma v_r l_r}{c^2},$$

Hydrodynamic Reynolds number $$Re=\frac{\rho v_r l_r}{\eta},$$

Magnetic Prandtl number $$Pm=\frac{4\pi\mu\sigma\eta}{\rho c^2},$$

Prandtl number $$Pr=\frac{\eta}{\kappa}$$

where the subscript 'r' designates reference values.

NUMERICAL ALGORITHM

Equations (11)–(14) represent a global system of highly coupled non-linear partial differential equations. For simplicity of computer programming the system is split into two systems. Equations (11)–(13) constitute the first system and equation (14) constitutes the second system. Each system is integrated by the explicit Runge–Kutta time-stepping method[7] in an alternating manner.

After transformation to generalized curvilinear non-orthogonal co-ordinates, the systems of governing equations can be written in fully conservative form as

$$\frac{\partial\mathbf{Q}}{\partial t}+\frac{\partial\mathbf{E}}{\partial\xi}+\frac{\partial\mathbf{F}}{\partial\eta}+\frac{\partial\mathbf{G}}{\partial\zeta}=D^2+\mathbf{D}. \tag{16}$$

For the flow field part of the global system the solution vector $\mathbf{Q}$, the flux vectors $\mathbf{E}$, $\mathbf{F}$ and $\mathbf{G}$ and the source vector $\mathbf{D}$ are given by

$$\mathbf{Q}=\frac{1}{J}\begin{bmatrix}0\\u\\v\\w\\\theta\end{bmatrix},\qquad \mathbf{E}=\frac{1}{J}\begin{bmatrix}U\\Uu+\xi_x p\\Uv+\xi_y p\\Uw+\xi_z p\\U\theta\end{bmatrix},\qquad \mathbf{F}=\frac{1}{J}\begin{bmatrix}V\\Vu+\eta_x p\\Vv+\eta_y p\\Vw+\eta_z p\\V\theta\end{bmatrix},$$

$$\mathbf{G}=\frac{1}{J}\begin{bmatrix}W\\Wu+\zeta_x p\\Wv+\zeta_y p\\Ww+\zeta_z p\\W\theta\end{bmatrix},\qquad \mathbf{D}=\begin{bmatrix}0\\d_2\\d_3\\d_4\\d_5\end{bmatrix}, \tag{17}$$

In order to integrate the system simultaneously and obtain a time-asymptotic solution, an artificial compressibility[8] term $\partial(p/\beta J)/\partial t$ is added to the solution vector, resulting in

$$\mathbf{Q}=\frac{1}{J}\begin{bmatrix} p/\beta \\ u \\ v \\ w \\ \theta \end{bmatrix}. \tag{25}$$

For the system of magnetic field equations the solution vector $\mathbf{Q}$, the flux vectors $\mathbf{E}$, $\mathbf{F}$ and $\mathbf{G}$ and the source vector $\mathbf{D}$ are given by

$$\mathbf{Q}=\frac{1}{J}\begin{bmatrix} H_1 \\ H_2 \\ H_3 \end{bmatrix}, \qquad \mathbf{E}=\frac{1}{J}\begin{bmatrix} H_1 U-u\hat{H}_\xi \\ H_2 U-v\hat{H}_\xi \\ H_3 U-w\hat{H}_\xi \end{bmatrix}, \qquad \mathbf{F}=\frac{1}{J}\begin{bmatrix} H_1 V-u\hat{H}_\eta \\ H_2 V-v\hat{H}_\eta \\ H_3 V-w\hat{H}_\eta \end{bmatrix},$$

$$\mathbf{G}=\frac{1}{J}\begin{bmatrix} H_1 W-u\hat{H}_\zeta \\ H_2 W-v\hat{H}_\zeta \\ H_3 W-w\hat{H}_\zeta \end{bmatrix}, \qquad \mathbf{D}=\mathbf{0}, \qquad \mathbf{S}=\frac{\mathbf{I}}{Rm}, \tag{26}$$

where $\mathbf{I}$ is the identity matrix of rank three.

The Runge-Kutta time-stepping method[7] given by

$$\begin{aligned} &\mathbf{Q}^0=\mathbf{Q}^t, \\ &\Delta\mathbf{Q}^k=-\alpha_k\Delta t\mathbf{R}^{k-1}, \quad k=1, 2, \ldots, K, \\ &\mathbf{Q}^{t+1}=\mathbf{Q}^t+\Delta\mathbf{Q}^K \end{aligned} \tag{27}$$

was used in the time integration of both systems. Here the residual vector is defined as

$$\mathbf{R}=\frac{\partial\mathbf{E}}{\partial\xi}+\frac{\partial\mathbf{F}}{\partial\eta}+\frac{\partial\mathbf{G}}{\partial\zeta}-D^2-\mathbf{D}+\frac{\delta}{8J\Delta t}\left(\frac{\partial^4}{\partial\xi^4}+\frac{\partial^4}{\partial\eta^4}+\frac{\partial^4}{\partial\zeta^4}\right)(J\mathbf{Q}). \tag{28}$$

The last term of the residual vector is the fourth-order artificial dissipation,[9] where δ is a user-specified small parameter and Δt is the time step. For the four-stage ($K=4$) Runge–Kutta method $\alpha_k=1/4$, $1/3$, $1/2$ and 1 respectively.

BOUNDARY CONDITIONS

The system of flow field equations is characterized by its hyperbolic nature. Therefore the boundary conditions have to be applied by considering the characteristic directions. The eigenvalues of the Jacobian matrix of the flux vector $\mathbf{E}$ are

$$\mathbf{L}=\mathrm{diag}(U-a, U+a, U, U, U), \tag{29}$$

where a is the equivalent speed of sound,

$$a=\sqrt{[U^2+\beta(\xi_x^2+\xi_y^2+\xi_z^2)]}. \tag{30}$$

At the inlet boundary one of the eigenvalues is negative. As a results, four boundary conditions should be imposed there. In this study the incoming velocity components u, v and w and the temperature θ are specified. The pressure p is computed from the characteristic equation. At the

exit boundary one boundary condition should be imposed. We specified the pressure, while the velocity components and the temperature were obtained by integrating the characteristic equations.

The application of the boundary conditions is given as follows.[10, 11] Premultiplying the equations by the similarity transformation matrix $\mathbf{M}_\xi^{-1}$ (in the ξ-direction), equation (27) results in the characteristic form of the equations. The equation corresponding to the negative eigenvalue is to be selected at the inlet, while at the exit the equations corresponding to positive eigenvalues are chosen. This selection procedure can be thought of as a matrix operation and we designate the operator as $\mathbf{L}$. If the boundary condition is given by $\mathbf{\Omega}$, then

$$\mathbf{\Omega}^{t+1} = \mathbf{\Omega}^t + \frac{\partial \mathbf{\Omega}}{\partial \mathbf{Q}} \Delta \mathbf{Q} \tag{31}$$

or

$$\frac{\partial \mathbf{\Omega}}{\partial \mathbf{Q}} \Delta \mathbf{Q} = -\mathbf{\Omega}^t, \tag{32}$$

and equation (32) is added to the transformed selected equations, that is

$$\left(\mathbf{L}\mathbf{M}_\xi^{-1} + \frac{\partial \mathbf{\Omega}}{\partial \mathbf{Q}} \right) \Delta \mathbf{Q} = -\alpha_k \Delta t \left(\mathbf{M}_\xi^{-1} \mathbf{R}^{k-1} + \frac{\mathbf{\Omega}^t}{\alpha_k \Delta t} \right). \tag{33}$$

At the inlet plane

$$\mathbf{L} = \operatorname{diag}(1, 0, 0, 0, 0), \tag{34}$$

$$\mathbf{\Omega} = [0, u - u_p, v - v_p, w - w_p, \theta - \theta_p]^T. \tag{35}$$

At the exit plane

$$\mathbf{L} = \operatorname{diag}(0, 1, 1, 1, 1), \tag{36}$$

$$\mathbf{\Omega} = [p - p_p, 0, 0, 0, 0]^T, \tag{37}$$

so that $\partial \mathbf{\Omega} / \partial \mathbf{Q} = \operatorname{diag}(\beta J, 0, 0, 0, 0)$. The subscript 'p' denotes the prescribed value and the superscript T designates the transpose of a vector. Along a solid wall the velocity components were set to zero. The pressure was deduced from the normal momentum equation, while the temperature was either specified or extrapolated depending on the boundary condition type (Neumann or Dirichlet boundary condition).

The system of magnetic field equations is also of hyperbolic type in time. The eigenvalues of the Jacobian matrix of this system are $\mathbf{L} = \operatorname{diag}(U, U, 0)$ in the ξ-direction. At the inlet plane, therefore, two components of the magnetic field vector are specified, while the axial component H_1 of the magnetic field vector is evaluated from the characteristic equation. The transformation matrix for the magnetic transport equations is given by

$$\mathbf{M}_\xi^{-1} = \begin{bmatrix} k_{23}v - k_{12}w & k_{31}w - k_{23}u & k_{12}u - k_{31}v \\ k_{23}w - k_{31}v & k_{31}u - k_{12}w & k_{12}v - k_{23}u \\ -\xi_x k_{123} & -\xi_y k_{123} & -\xi_z k_{123} \end{bmatrix}, \tag{38}$$

where

$$k_{12}=\xi_3^2-\xi_x\xi_y, \qquad k_{23}=\xi_1^2-\xi_y\xi_z, \qquad k_{31}=\xi_2^2-\xi_z\xi_x, \qquad k_{123}=k_{12}+k_{23}+k_{31}, \tag{39}$$

$$\mathbf{L}=\mathrm{diag}(1, 1, 0), \tag{40}$$

$$\mathbf{\Omega}=[H_2-H_{2p}, H_3-H_{3p}, 0]^T. \tag{41}$$

At the exit plane all three variables are updated by integrating the governing equations.

Let $\langle\ \rangle$ denote a jump across the boundary. If the wall is a perfect conductor, the tangential component of the magnetic field experiences the discontinuity but the normal component should be continuous:

$$\mathbf{n}\times\langle\mathbf{E}\rangle=0, \qquad \mathbf{n}\cdot\mathbf{H}=0. \tag{42}$$

If the wall is a perfect insulator, the boundary condition takes the simpler form

$$\langle\mathbf{H}\rangle=0. \tag{43}$$

STABILITY ANALYSIS

Consider a model system of equations

$$\frac{\partial\mathbf{Q}}{\partial t}+\mathbf{A}\frac{\partial\mathbf{Q}}{\partial x}=\mathbf{0}. \tag{44}$$

The Runge–Kutta method with the split approach can be thought of as a $2K$-stage multistage method, that is

$$\mathbf{Q}^k=\mathbf{Q}^0-\alpha_k\Delta t\begin{bmatrix} a_{11} & a_{12} \\ 0 & 0 \end{bmatrix}\frac{\partial\mathbf{Q}^{k-1}}{\partial x} \qquad \text{for } k=1, \ldots, K,$$

$$\mathbf{Q}^k=\mathbf{Q}^K-\alpha_k\Delta t\begin{bmatrix} 0 & 0 \\ a_{21} & a_{22} \end{bmatrix}\frac{\partial\mathbf{Q}^{k-1}}{\partial x} \qquad \text{for } k=K+1, \ldots, 2K,$$

with

$$\alpha_{k+K}=\alpha_k. \tag{45}$$

In other words, the flow field variables (p, u, v, w) are updated first via a four-stage Runge–Kutta scheme. This was followed by the update of the magnetic field vector components (H_1, H_2, H_3) also via a four-stage Runge–Kutta scheme. Thus the variables are not updated individually in a predetermined order as in the case of certain pressure–velocity field update codes. If the provisional amplification matrix $\mathbf{G}_k$ for the first K stages of the Runge–Kutta scheme is defined as

$$\mathbf{Q}^k=\mathbf{G}_k\mathbf{Q}^0, \tag{46}$$

then we have the recursion formula for the provisional amplification matrix

$$\tilde{\mathbf{G}}_k=\mathbf{I}-\alpha_k\Delta t\tilde{\mathbf{N}}_1\mathbf{G}_{k-1} \quad \text{for } k=1, \ldots, K, \tag{47}$$

where

$$\tilde{\mathbf{G}}_0=\mathbf{I}, \qquad \tilde{\mathbf{N}}_1=\mathrm{i}\frac{\sin(\kappa\Delta x)}{\Delta x}\begin{bmatrix} a_{11} & a_{12} \\ 0 & 0 \end{bmatrix}. \tag{48}$$

Similarly, define the provisional amplification matrix $\tilde{\mathbf{G}}_k$ for the second K stages as

$$\tilde{\mathbf{G}}_k = \mathbf{I} - \alpha_k \Delta t \tilde{\mathbf{N}}_2 \mathbf{G}_{k-1} \quad \text{for } k = K+1, \ldots, 2K, \tag{49}$$

where

$$\tilde{\mathbf{G}}_K = \mathbf{I}, \qquad \tilde{\mathbf{N}}_2 = \mathrm{i} \frac{\sin(\kappa \Delta x)}{\Delta x} \begin{bmatrix} 0 & 0 \\ a_{21} & a_{22} \end{bmatrix}. \tag{50}$$

The amplification factor of the Runge–Kutta method for the split approach can be found as

$$\mathbf{G} = \mathbf{G}_K \tilde{\mathbf{G}}_{2K} = P(\tilde{\mathbf{N}}_1)\, P(\tilde{\mathbf{N}}_2), \tag{51}$$

where P designates a polynomial. Thus the amplification matrices for the split approach and the unsplit approach are equal

$$\mathbf{G}_{\text{split}} = P(\tilde{\mathbf{N}}_1, \tilde{\mathbf{N}}_2) = \mathbf{G}_{\text{unsplit}}. \tag{52}$$

In general, if we split the system of equations into a number of systems and if the stability conditions for each system are satisfied, then the complete system remains stable. It should be pointed out that in principle it should be possible to use different time steps for each set of equations. Nevertheless, determining and optimizing two separate time steps for the two systems of equations was not attempted in this work.

COMPUTATIONAL RESULTS

Computer codes that we have developed, although allowing for arbitrary configurations, have been tested for accuracy against simple flow problems for which analytical solutions are known. The first test case is the two-dimensional Hartman flow, which is equivalent to the Poiseuille flow in fluid dynamics. An H-type orthogonal grid of 50×20 cells was used in this computation (Figure 1). The length of the channel was 15 times the half-height of the channel. The y-component of the magnetic field H_0 on the solid walls was kept constant. As a result of the Lorentz force, the velocity profile is flatter than the velocity profile without the magnetic field. The hydrodynamic Reynolds number Re based on the average velocity and the half-height of the channel was $Re = 10$, while the magnetic Reynolds number was $Rm = 10$. The Hartman number based on the vertical uniformly imposed magnetic field and the half-height of the channel was $Ht = 5$. An artificial compressibility coefficient $\beta = 10$ was found through numerical experimentation to give the best convergence. All computer runs were performed with CFL = 2·8, which is the maximum allowable value for this type of explicit algorithm. Different values of β have been shown to influence only the convergence rate.[12]

In this computation the influence of the buoyancy force was neglected. Therefore the energy equation was decoupled from the rest of the equations. The imposed inlet velocity profile was that of Poiseuille flow. Since both Reynolds numbers are small, the flow develops fully over a short distance (Figure 2). The pressure gradient becomes constant near the exit. Figure 3 compares the computed velocity profile with that of an analytical solution.[5] In Figure 4 the computed induced

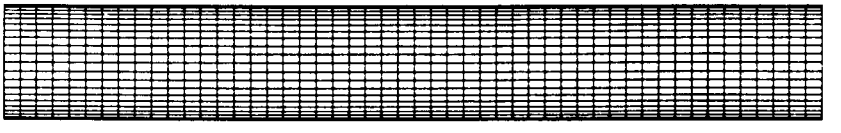

Figure 1. H-type computational grid used for two-dimensional Hartman flow

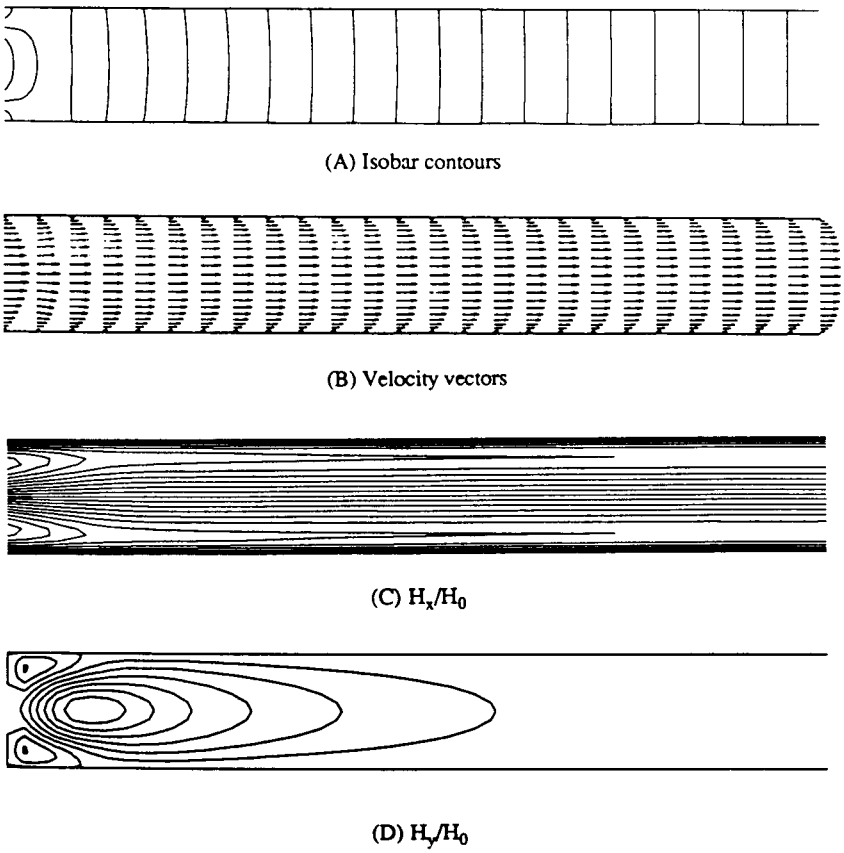

Figure 2. Solutions of two-dimensional Hartman flow

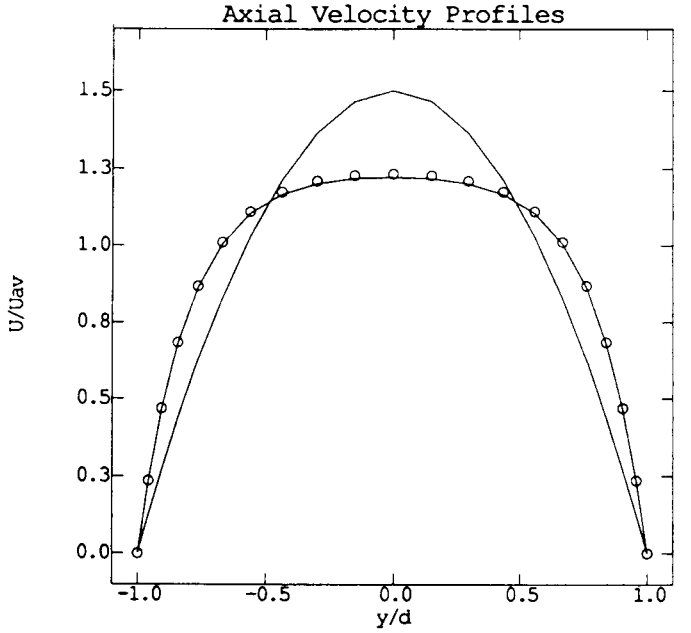

Figure 3. Axial velocity component at the exit (two-dimensional Hartman flow): upper curve, inlet velocity; lower curve, computations; circles, analytic solution

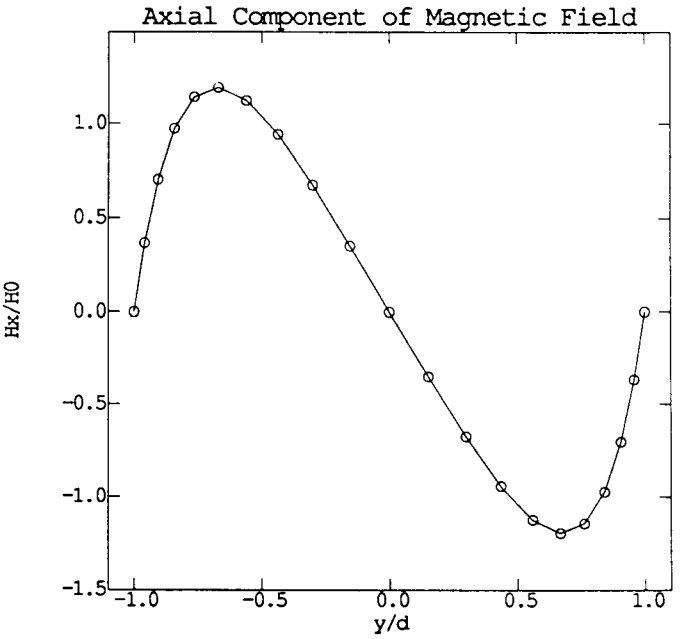

Figure 4. Axial magnetic field component at the exit (two-dimensional Hartman flow): curve, computations; circles, analytic solution

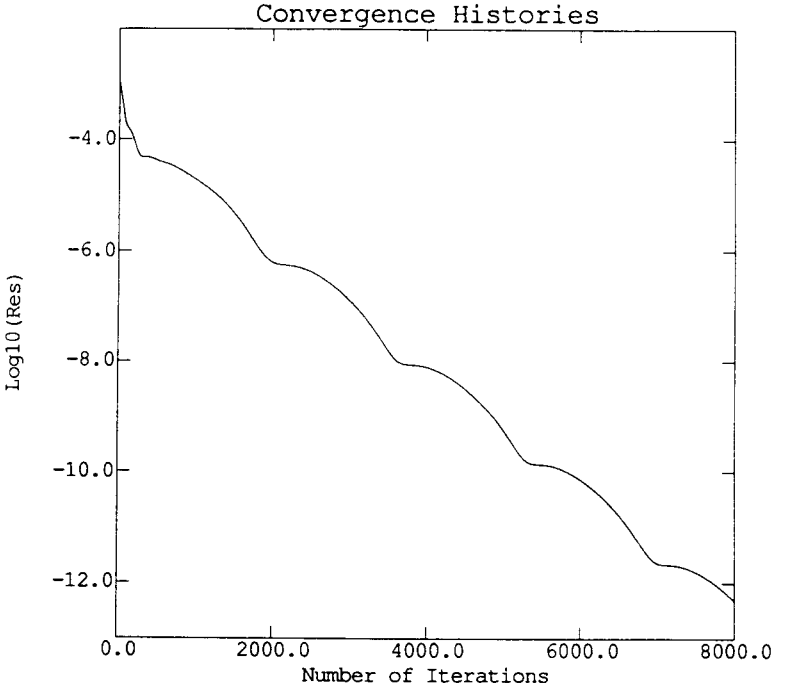

Figure 5. Convergence history (two-dimensional Hartman flow)

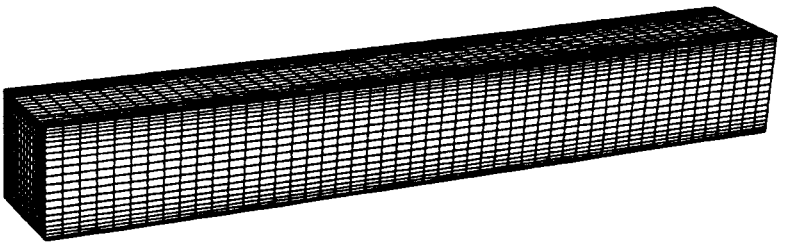

Figure 6. Computational domain for three-dimensional Hartman flow

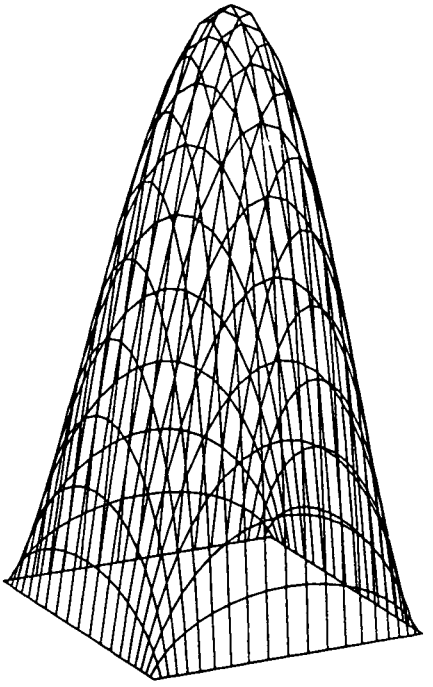

Figure 7. Inlet velocity profile

axial component of the magnetic field is compared with the analytic solution, showing excellent agreement. The relative error compared to the analytic solution is about 0·88% for the axial velocity component and 0·04% for the axial component of the magnetic field. The convergence history of the test case is shown in Figure 5. The code runs at 14 μs per grid point per iteration on the Cray II computer.

The next test case is an equivalent Hartman flow in three dimensions. The computational domain was discretized with $50 \times 20 \times 20$ rectangular clustered cells (Figure 6). Both hydrodynamic and magnetic Reynolds numbers were 10. The value of the artificial compressibility coefficient was $\beta = 10$. Figure 7 shows the prescribed inlet velocity profile, which is a fully developed laminar flow profile without the magnetic field. Carpet plots of the analytic and computed x-component of the velocity vector are shown in Figure 8. The maximum relative error of the computed solution is 0·73%. Figure 9 shows the analytic and computed x-component of the magnetic field. The computed solution deviates by less than 0·74% from the analytic solution.

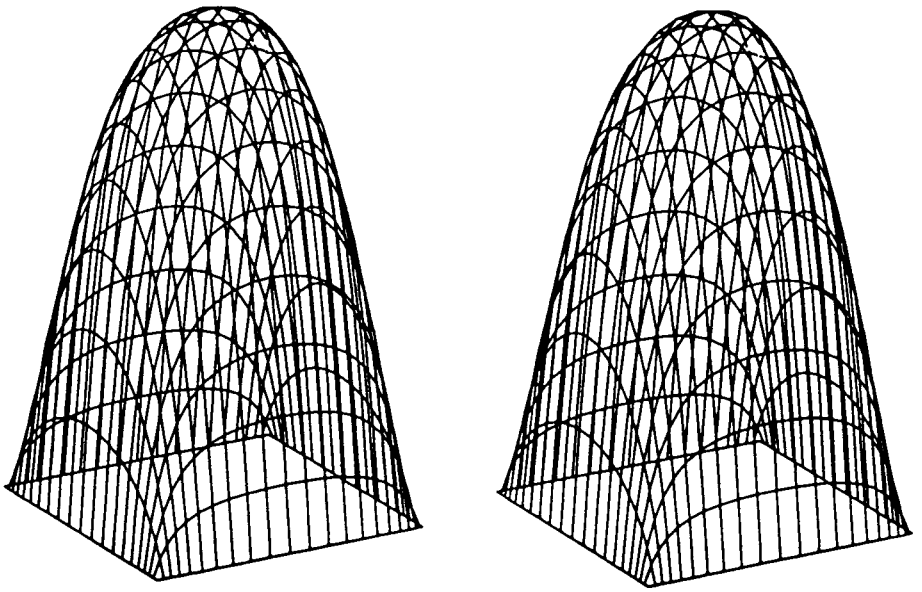

(A) Analytic solution (B) Computed solution

Figure 8. Axial component velocity profile

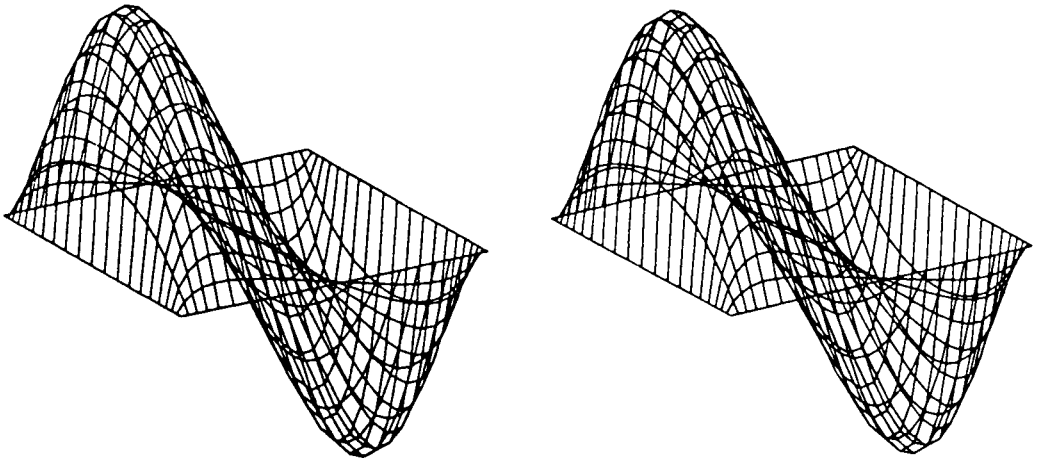

(A) Analytic solution (B) Computed solution

Figure 9. Axial component of the magnetic field vector

For completeness, the analytic solution[13] of the three-dimensional Hartman flow is given here:

$$\frac{u}{u_{av}}=\frac{4}{\pi^3}\left(\frac{b}{a}\right)^2 Re\,\hat{k}\sum_{n\,\mathrm{odd}}^{\infty}\left\{1-\cosh\left[\frac{Ht}{2}\left(\frac{y}{a}-1\right)\right]\sinh\left(\frac{Hty}{2a}\right)\sinh^{-1}\left(\frac{H}{2}\right)\right.$$
$$\left.-\cosh\left(\frac{Hty}{2a}\right)\sinh\left[\frac{Ht}{2}\left(\frac{y}{a}-1\right)\right]\sinh^{-1}\left(\frac{H}{2}\right)\right\}\frac{\sin(n\pi z/b)}{n^3}. \tag{53}$$

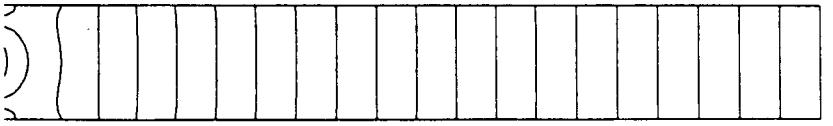

(A) Isobar contours

(B) Velocity vectors

(C) H_x/H_0

(D) H_y/H_0

Figure 10. Solutions of three-dimensional Hartman flow ($z/a=0{\cdot}5$)

The H_1-component with the given H_2-component is

$$\frac{H_1}{H_2}=\frac{4}{\pi^3}\left(\frac{b}{a}\right)^2\frac{RmRe}{Ht}\hat{k}\sum_{n\,\mathrm{odd}}^{\infty}\left\{1-\sinh\left[\frac{Ht}{2}\left(\frac{y}{a}-1\right)\right]\sinh\left(\frac{Hty}{2a}\right)\sinh^{-1}\left(\frac{H}{2}\right)\right.$$
$$\left.-\sinh\left(\frac{Hty}{2a}\right)\sinh\left[\frac{Ht}{2}\left(\frac{y}{a}-1\right)\right]\sinh^{-1}\left(\frac{H}{2}\right)\right\}\frac{\sin(n\pi z/b)}{n^3}. \tag{54}$$

Here a and b are the width and height of the duct respectively, while

$$\frac{1}{Re}=8\hat{k}\left(\frac{b}{a}\right)^2\sum_{n\,\mathrm{odd}}^{\infty}\frac{1}{n^4}\left[1+\left(\frac{b}{a}\right)^2\frac{H}{(n\pi)^2}\frac{\cosh(H/2)-\cosh(Ht/2)}{\sinh(H/2)}\right], \tag{55}$$

where the hydrodynamic and magnetic Reynolds numbers, the Hartman number and the normalized pressure gradient are given by

$$Re=\frac{\rho u_{\mathrm{av}}a}{\eta},\qquad \hat{k}=\frac{a}{\rho u_{\mathrm{av}}^2}\frac{\partial p}{\partial x},\qquad Ht=\mu aH_2\sqrt{\left(\frac{\sigma}{c^2\eta}\right)},\qquad Rm=\frac{4\pi\mu\sigma u_{\mathrm{av}}a}{c^2}. \tag{56}$$

Figure 10 shows the pressure, the developing velocity profile and the axial and vertical components of the magnetic field vector normalized with the applied magnetic strength along the vertical midplane ($z/a = 0{\cdot}5$). Both flow field and magnetic field develop within two duct heights downstream from the inlet. The convergence history is plotted in Figure 11. For this case the code was executed at 15 μs per grid point per iteration on the Cray Y-MP computer.

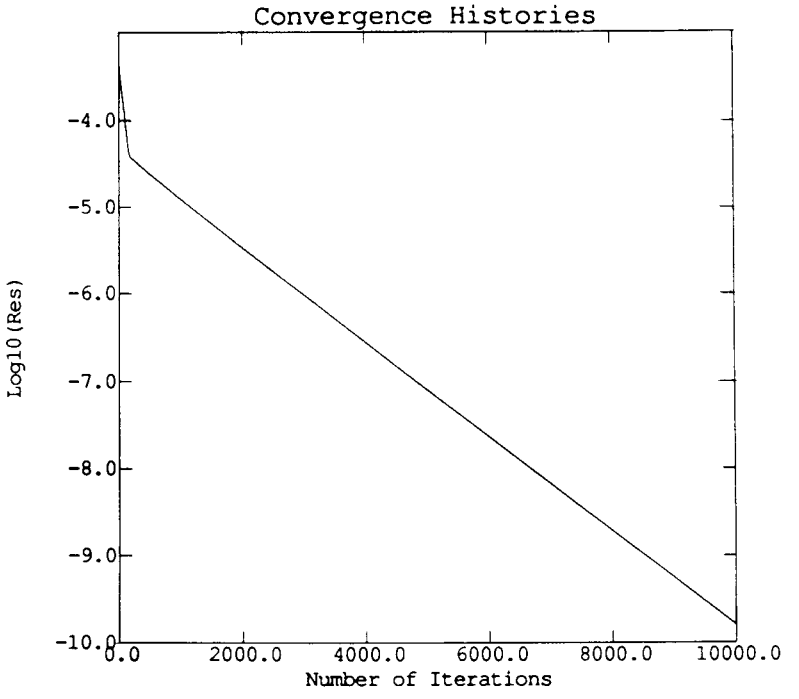

Figure 11. Convergence history (three-dimensional Hartman flow)

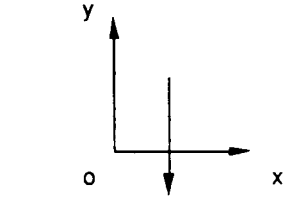

$\vec{g}$ (gravity) and $\vec{H}$ (imposed)

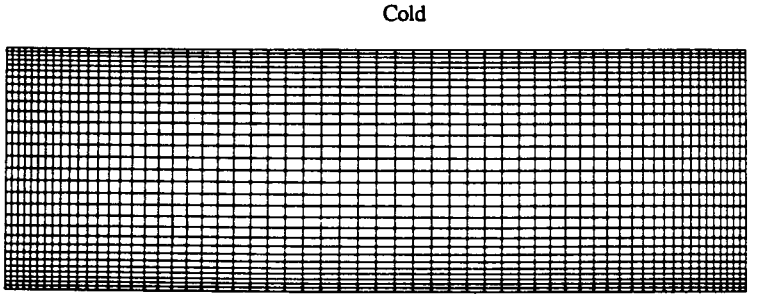

Figure 12. Closed container: computational grid of 60 × 30 cells

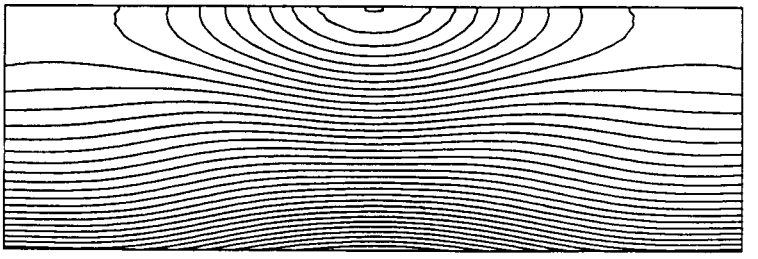

Isobars (without magnetic field)

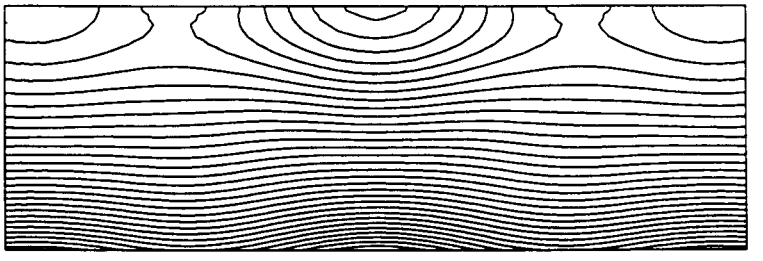

Isobars (with magnetic field)

Figure 13. Isobar contours

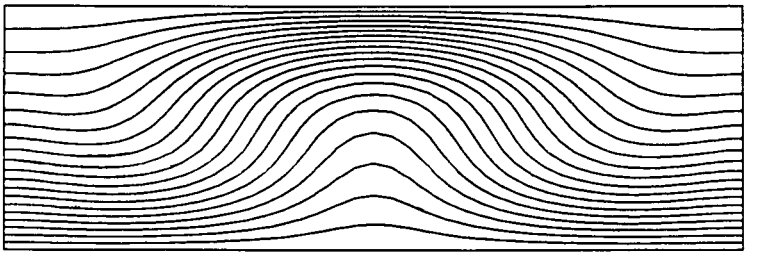

Isotherms (without magnetic field)

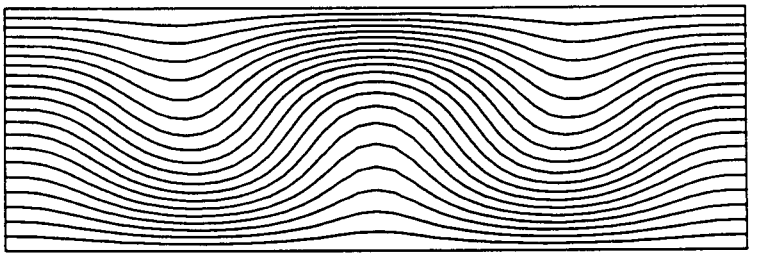

Isotherms (with magnetic field)

Figure 14. Isothermal contours

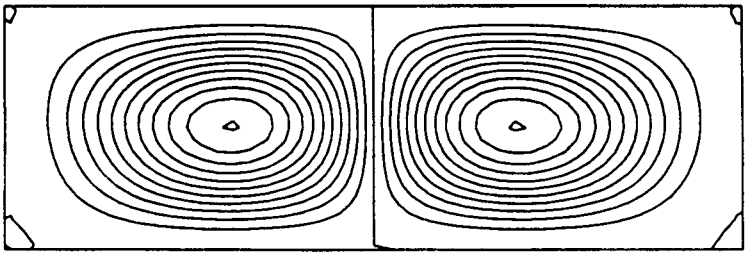

Streamlines (without magnetic field)

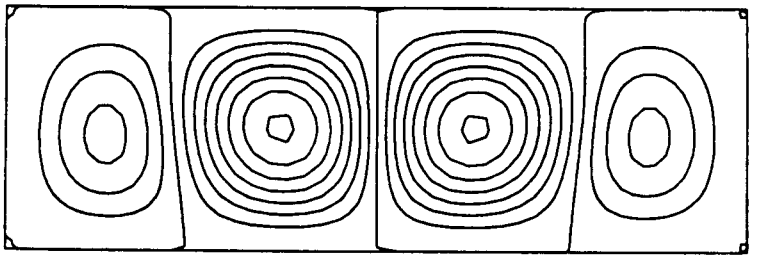

Streamlines (with magnetic field)

Figure 15. Streamlines

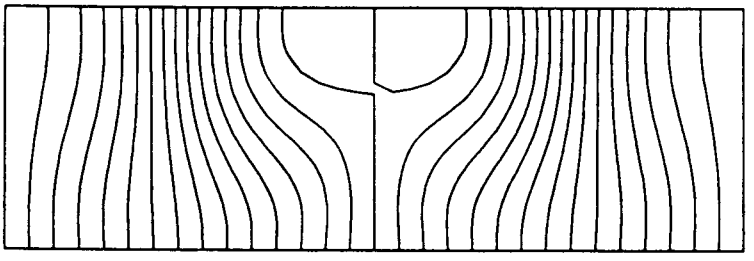

Figure 16. Lines of forces

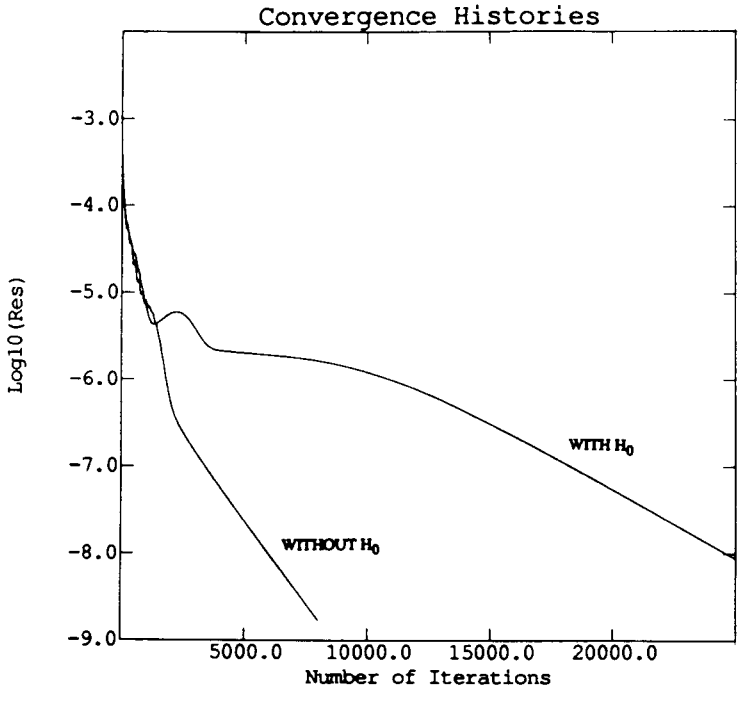

Figure 17. Convergence histories

The next example is the two-dimensional Bènard cell problem under the influence of a magnetic field. The imposed magnetic field is parallel to the gravitation. To study the relative influence of the magnetic field, the computations were done both with and without the applied magnetic field. The Hartman number was $Ht = 5$ and the Grashof number was $\mathrm{Gr} = 3000$, with the bottom wall hot, the top wall cold and the side walls thermally insulated. Since there is no reference velocity, the reference velocity was obtained by equating the magnitude of the buoyancy term to that of the viscous term.[14] An orthogonal grid of 60×30 cells was used in this computation (Figure 12). An artificial compressibility coefficient $\beta = 1$ was used for both computations since this value was found to give the best convergence rate. Both the magnetic Prandtl number and the hydrodynamic Prandtl number were unity. Although no artificial dissipation was

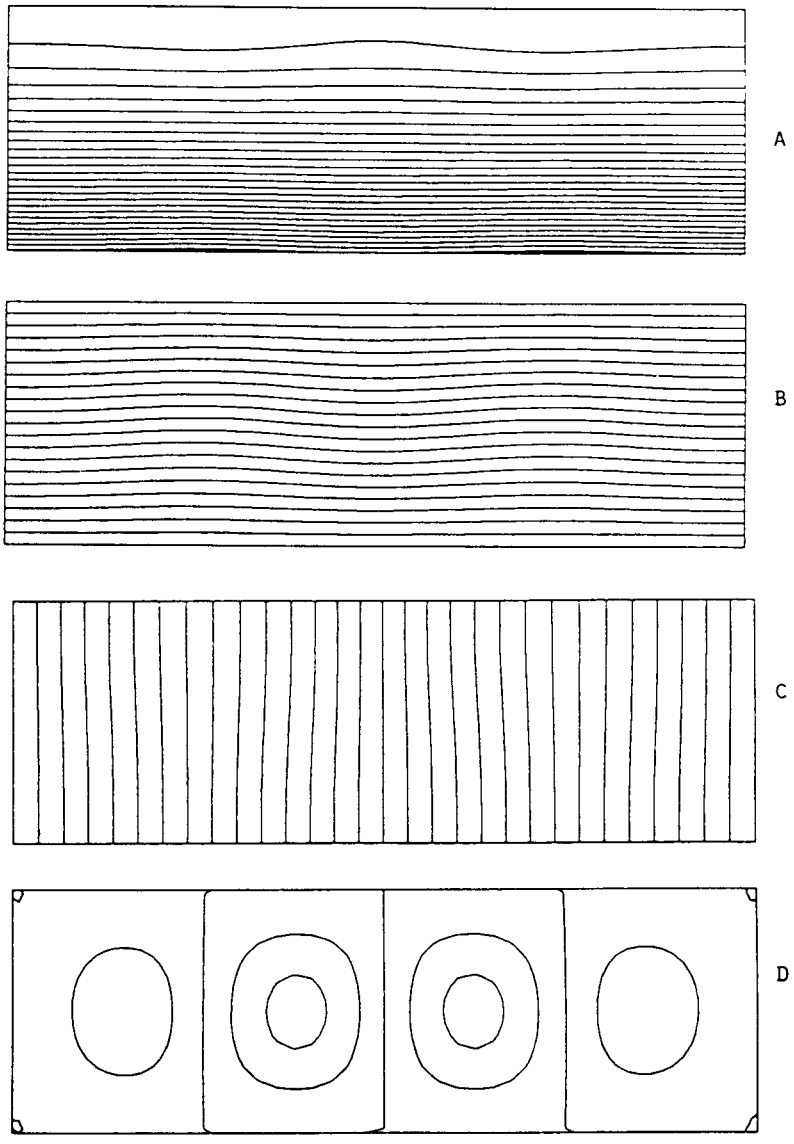

Figure 18. Interaction of a thermally induced flow and a strong magnetic field with $Ht = 10$: A, isobars; B, isotherms; C, magnetic force lines; D, streamlines

added, smooth solutions were obtained. The pressure along the solid wall was computed from the normal momentum equation.[14]

Figure 13 shows isobar contours for computations with and without the applied magnetic field. As can be seen, the usual boundary condition for pressure, $\partial p/\partial n = 0$, would have given erroneous results both with and without the influence of the magnetic field. The isothermal contours for both cases are plotted in Figure 14. Figure 15 represents the streamlines for both cases. With the applied magnetic field the strength of the vortices was weakened and the cells were elongated, which was predicted by Chandrasekhar[6] through a hydrodynamic linear stability analysis. Figure 16 depicts the lines of magnetic forces. They would be straight vertical lines without the flow induced by buoyancy. Figure 17 shows the convergence histories for both cases. It is noticeable that the convergence rate for the case with the applied magnetic field is much slower than without the magnetic field. It was found that with a Hartman number of 10 the circulatory motions from the thermal instability were damped significantly (Figure 18). Although a thorough parametric study has not been performed, it is believed that the critical Hartman number beyond which the circulation would be entirely suppressed at a Grashof number of 3000 is between 10 and 15.

CONCLUSIONS

Using the explicit approach, the governing equations of magnetohydrodynamics were solved with high accuracy. The stability analysis for a sample system shows that if each individual system satisfies the stability conditions, the complete system is stable. Numerical examples including two- and three-dimensional Hartman flow were computed. Recirculating flow generated by thermally induced buoyancy was suppressed by the magnetic field.

ACKNOWLEDGEMENTS

The lead author would like to thank the Center for Cell Research at Penn State University for partially supporting this work and Mr. Robert Kunz for useful discussions. Computations were performed on the NAS facility at NASA Ames Research Center. Computing time was provided by Dr. Robert Stubbs of NASA Lewis Research Center. Graphics were produced on equipment donated by Apple Computer Co., Inc.

REFERENCES

1. E. D. Doss, G. S. Argyropoulos and S. T. Demetriades, 'Two-dimensional flow inside MHD ducts with transverse asymmetries', *AIAA J.*, **13**(5), 545–546 (1975).
2. L. A. Feldman and J. E. Burkhalter, 'Numerical solutions of transient MHD phenomena', *AIAA J.*, **17**(3), 227–228, (1979).
3. F. Grasso and C. G. Speziale, 'Supersonic flow computations by two-equation turbulence modelling', *AIAA Paper 89-1951*, 1989.
4. R. F. Kunz and B. Lakshminarayana, 'Computation of supersonic and low subsonic cascade flows using an explicit Navier–Stokes technique and k–ε turbulence model', in M.-S. Lin (ed.), *Proc. CFD Symp. in Aeropropulsion*, NASA Lewis Research Center, Cleveland, OH, 24–26 April 1990; NASA CP-3078, pp. 163–201.
5. A. Jeffrey, *Magnetohydrodynamics, University Mathematical Texts 33*, Oliver & Boyd, Edinburgh, 1966.
6. S. Chandrasekhar, *Hydrodynamic and Hydromagnetic Stability*, Dover, New York, 1961.
7. A. Jameson, W. Schmidt and E. Turkel, 'Numerical solutions of the Euler equations by finite volume methods using Runge–Kutta time-stepping scheme', *AIAA Paper 81-1259*, Palo Alto, CA, June 1981.
8. A. J. Chorin, 'A numerical method for solving incompressible viscous flow problems', *J. Comput. Phys.*, **2**, 12–26 (1967).
9. J. L. Steger and P. Kutler, 'Implicit finite-difference procedure for the computation of vortex wakes', *AIAA J.*, **15**(4), 581–590 (1977).
10. S. E. Rogers, D. Kwak and J. L. C. Chang, 'INS3D—an incompressible Navier–Stokes code in generalized three-dimensional coordinates', *NASA TM-100012*, November 1987.

11. D. Pan and S. Chakravarthy, 'Unified formulation for incompressible flows', *AIAA Paper 89-0122, 27th Aerospace Sciences Meeting*, Reno, NV, 9–12 January 1989.
12. S. Lee and G. S. Dulikravich, 'Performance analysis of DMR method for acceleration of iterative algorithms', *AIAA Paper 91-0241, Aerospace Sciences Meeting*, Reno, NV, 7–10 January 1991.
13. G. W. Sutton and A. Sherman, *Engineering Magnetohydrodynamics*, McGraw-Hill, New York, 1965, pp. 334–381.
14. S. Lee, 'Acceleration of iterative algorithms for Euler and Navier–Stokes equations', *Ph.D. Thesis*, Department of Aerospace Engineering, The Pennsylvania State University, May 1990.